

# The importance of ice sheet growth and retreat on magmatism and mantle CO<sub>2</sub> flux

John J. Armitage<sup>1</sup>, David J. Ferguson<sup>2</sup>, Kenni D. Petersen<sup>3</sup>, and Timothy T. Creyts<sup>4</sup>

<sup>1</sup>Dynamique des Fluides Géologiques, Institut de Physique du Globe de Paris, Paris, France

<sup>2</sup>School of Earth and Environment, University of Leeds, Leeds, U.K.

<sup>3</sup>Department of Geoscience, University of Aarhus, Aarhus, Denmark

<sup>4</sup>Lamont-Doherty Earth Observatory, Columbia University, U.S.A

## Key Points:

- We combine a new history of Icelandic ice-cover with a forward model of magma generation.
- Magmatism and CO<sub>2</sub> outgassing is influenced by both the rate of deglaciation and, importantly, the preceding growth of the ice sheet.
- Peak mantle CO<sub>2</sub> flux is non-linearly related to magmatic eruption rates.

15 **Abstract**

16 Climate cycles may significantly affect the eruptive behavior of terrestrial volcanoes due  
 17 to pressure changes caused by glacial loading, which raises the possibility that climate  
 18 change may modulate CO<sub>2</sub> degassing via volcanism. In Iceland, magmatism is likely to  
 19 have been influenced by glacial activity. To explore if deglaciation therefore impacted  
 20 CO<sub>2</sub> flux we coupled a model of glacial loading over the last ~120 ka to melt generation  
 21 and transport. We find that a nuanced relationship exists between magmatism and glacial  
 22 activity. Enhanced CO<sub>2</sub> degassing happened prior to the main phase of late-Pleistocene  
 23 deglaciation, and it is sensitive to the duration of the growth of the ice sheet entering  
 24 into the LGM, as well as the rate of ice loss. Ice sheet growth depresses melting in the  
 25 upper mantle, creating a delayed pulse of CO<sub>2</sub> out-gassing as the magmatic system re-  
 26 covers from the effects of loading.

27 **1 Introduction**

28 Evidence from several tectonic settings indicates that glaciated volcanic systems  
 29 respond to changing ice volumes (Glazner, Manley, Marron, & Rojstaczer, 1999; Jellinek,  
 30 Mange, & Saar, 2004; Jull & McKenzie, 1996; MacLennan, Jull, McKenzie, Slater, & Grönvöld,  
 31 2002; Rawson et al., 2016; Sigvaldsson, Annertz, & Nilsson, 1992), and suggests there was  
 32 a widespread volcanic response to late-Pleistocene ice retreat (Huybers & Langmuir, 2009).  
 33 The most compelling evidence for climate-coupled volcanism comes from Iceland, where  
 34 changes in early Holocene lava volumes and magma chemistry are consistent with de-  
 35 pressurization during glacial unloading (Jull & McKenzie, 1996; MacLennan et al., 2002;  
 36 Sinton, Grönvöld, & Saemundsson, 2005). Magma generation here occurs due to pressure-  
 37 release melting, as the mantle up-wells beneath rift zones. Although the net change in  
 38 overburden pressures from variations in ice cover red have been relatively small, the high  
 39 rates of change associated with glacial activity can produce significant short-term fluc-  
 40 tuations in magmatic output (Jull & McKenzie, 1996; Pagli & Sigmundsson, 2008; Schmidt  
 41 et al., 2013), similar to those hypothesised to occur at ocean ridges due to sea-level var-  
 42 iation (Burley & Katz, 2015; Crowley, Katz, Huybers, Langmuir, & Park, 2015; Huybers  
 43 & Langmuir, 2009; Lund & Asimow, 2011). Carbon readily partitions into magmas dur-  
 44 ing partial melting (Rosenthal, Hauri, & Hirschmann, 2015) and is released as a CO<sub>2</sub> rich  
 45 fluid/vapour as the magma ascends through the crust, making volcanism the primary  
 46 pathway for transporting carbon from the Earth's mantle to the atmosphere (Dasgupta  
 47 & Hirschmann, 2010). However, carbon does not enter the melt uniformly during par-  
 48 tial melting and is concentrated in early formed magma and does not enter the melt uni-  
 49 formly over time. Therefore the extent to which glacially driven changes in primary magma  
 50 generation alter the flux of CO<sub>2</sub> depends on where in the melting column melt produc-  
 51 tion is enhanced (or suppressed), the rate of melt transport, and the history of ice sheet  
 52 growth and retreat.

53 Global data sets of the number of volcanic eruptions throughout the Pleistocene  
 54 would suggest there is a correlation between climatic change and volcanism (Huybers  
 55 & Langmuir, 2009), yet data resolution makes testing this association difficult. It is thought  
 56 that CO<sub>2</sub> and the trace element Nb have a relatively similar behaviour during decom-  
 57 pression melting (Saal, Hauri, Langmuir, & Perfit, 2002), and as such Nb compositions  
 58 can be used to gauge the quantity of CO<sub>2</sub> erupted. In Iceland there are just over 300 pub-  
 59 lished dated analysis of the Nb composition of Pleistocene lavas (Eason, Sinton, Grönvöld,  
 60 & Kurz, 2015; Gee, Taylor, Thirwall, & Murton, 1998). This is arguably the most com-  
 61 plete geochemical record within a region that experienced significant Pleistocene deglaci-  
 62 ation. In this study we take a new approach, and use a high resolution model of ice sheet  
 63 history to drive a forward model of melt generation and transport. We predict the change  
 64 in eruption rates and melt composition as a function of the changing surface load. We  
 65 validate the model predictions against steady state melt thickness and validate the pre-  
 66 dicted melt porosity against the seismic structure imaged below Iceland. We subsequently

67 explore under what conditions climate and magmatism might be related, and the im-  
68 plications for CO<sub>2</sub> degassing.

## 69 **2 Methods**

### 70 **2.1 Modelling of Melt Generation and Transport**

71 To investigate the impact of glacial activity on melt productivity, melt composi-  
72 tion, and CO<sub>2</sub> flux, we used a model of magma generation and transport coupled to a  
73 model of the flexure of a viscoelastic beam for the response to change in load due to the  
74 ice sheet history (see Supplementary Material). The coupled model consists of a flexu-  
75 ral model of the surface displacement due to the changing surface load as the ice sheet  
76 changes in thickness. This model of surface displacement is then coupled to either a 1D  
77 vertical column or a 2D corner flow model where the flow of the mantle is prescribed at  
78 either an upwelling rate of 10 or 20 mm yr<sup>-1</sup>, or lateral spreading rate of 10 mm yr<sup>-1</sup>. We  
79 use these two upwelling rates to cover the uncertainty in the exact rate of vertical as-  
80 cent the mantle below Iceland due to mantle buoyancy. The upwelling column is per-  
81 turbed by the displacement due to loading, where the viscoelastic decay time of the load  
82 is set to 1000 yrs. Carbon partitioning into the melt is assumed to be governed by the  
83 coefficients derived by (Rosenthal et al., 2015). We use a mantle source composition for  
84 Nb of 1.627 ppm, which is intermediate between the end-member sources for Icelandic  
85 melts identified by (Shortle & MacLennan, 2011). To approximate the melting of the mul-  
86 tiple source lithologies we chose a solidus-depletion gradient of 600 °C which is interme-  
87 diate between that of melting experiments on depleted mantle, 900 °C (Wasylenski, Baker,  
88 Kent, & Stopler, 2003) and fertile mantle 300 °C (Scott, 1992).

89 The surface expression of partial melting to glacial loading/unloading is influenced  
90 primarily by the rate at which the melt percolates through the mantle (Burley & Katz,  
91 2015). To constrain the permeability of melt transport, we examined the effects of vary-  
92 ing the permeability coefficient on the seismic properties of the mantle produced by our  
93 1-D model. The thermal structure and porosity was converted to S-wave velocities, as-  
94 suming that melt reduces the velocity by 7.9 % per percent porosity (Hammond & Humphreys,  
95 2000) and including the effects of attenuation (Goes, Armitage, Harmon, Huismans, &  
96 Smith, 2012). Recent joint inversion of teleseismic and ambient noise Rayleigh waves in  
97 Iceland would suggest that the S-wave velocity is between 4 and 3.8 km s<sup>-1</sup> at depths  
98 of 50 to 150 km (Harmon & Rychert, 2016) (Figure 1). We find that the permeability  
99 coefficient,  $k_0$ , needs to be relatively high ( $10^{-5}$  m<sup>2</sup>) giving a permeability,  $k_\phi = k_0 \phi^3$   
100 (where  $\phi$  is porosity), of the order of  $10^{-14}$  m<sup>2</sup> ( $\phi \approx 0.001$ ; Figure 1), because other-  
101 wise porosity would be too large and the S-wave velocity would decrease below the ob-  
102 served values. This permeability is an order of magnitude higher than the upper range  
103 used to explore how sea-level change might influence mid-ocean ridge (MOR) magma-  
104 tism (Burley & Katz, 2015; Crowley et al., 2015), and suggests rates of magmatic ascent  
105 of the order of 10 m yr<sup>-1</sup>, in agreement with MacLennan et al. (2002). Previously it has  
106 been suggested that delays in signal propagation from the zone of partial melting at MORs  
107 to the surface might be of the order of a Milankovitch-scale period, 40 kyr (Huybers &  
108 Langmuir, 2017). However, the high permeability required to match the seismic obser-  
109 vations from Iceland implies a magmatic system that much more rapidly responds to change  
110 in melting conditions, consistent with the fast transport rates estimated from U-series  
111 isotope studies (Elliot & Spiegelman, 2014).

### 112 **2.2 Glacial Forcing Throughout the Pleistocene**

113 Iceland experienced extensive ice-cover during the last glacial period (Patton, Hub-  
114 bard, Bradwell, & Schomacker, 2017), with maximum thicknesses in the center of the  
115 island of ~ 2km attained by ~23 ka (Figure 2a and b). Deglaciation after the LGM oc-  
116 curred at a varying rate, and was discontinuous. For example, a stage of re-advance oc-

117 curred during the colder climate of the Younger Dryas (11.7-12.9 ka) (Nordahl & Ingólfsson,  
 118 2015). The final phase of deglaciation was particularly rapid, with the main volcanic zones  
 119 being largely ice free by  $\sim$ 10 ka (Figure 2a). The most uncertain period of the glacial  
 120 history is the pre-LGM growth of the ice sheet. To create the ice sheet histories shown  
 121 in Figure 2b and Figure 3a we calibrated the ice volume since the LGM against the North  
 122 Greenland Ice Core Project (NGRIP)  $\delta^{18}\text{O}$  record, and Quaternary sea-level curves as-  
 123 suming a linear correlation between these three signals (see Supplementary Material Text  
 124 S1). We focus on two scenarios: M1, based on the ICE-5G sea-level curves (Peltier, 2004),  
 125 and M2, based on the sea-level curves of Pico, Creveling, and Mitrovica (2017) (Figure  
 126 S2).

### 127 3 Results

#### 128 3.1 Effect of glacial loading and unloading

129 We force our melt model with the 120 ka glacial history after a 5 Myr model wind-  
 130 up to steady state (model M1, Figure 2b) and using a single value for the ice thickness  
 131 at each time-step, therefore neglecting the effects of the distal parts of the ice sheet on  
 132 melting beneath the rift margins. The model predicts peaks in magmatic output and  $\text{CO}_2$   
 133 flux as pressure changes due to loading and unloading impact the melt production rate  
 134 (Figure 2). The response of the magmatic system to changes in ice cover varies depend-  
 135 ing on the mantle upwelling rate, the rate-of-change in ice sheet thickness, and the prior  
 136 ice sheet history. Glacial loading suppresses melt production (Jull & McKenzie, 1996),  
 137 leading to a decline in magma supply (see Supplementary Material, Figure S3). For ex-  
 138 ample during the period between 35 and 15 ka, the growth of the ice sheet reduces erup-  
 139 tion rates below 5 km of melt per Myr (Figure 2c). The recovery from this loading oc-  
 140 curs initially in the deepest part of the system as this region is perturbed the least. Re-  
 141 covery is also faster if the mantle upwelling rate is higher, where an upwelling rate of  $20 \text{ mm yr}^{-1}$   
 142 is more responsive than the equivalent  $10 \text{ mm yr}^{-1}$  model (Figure 2b). Higher rates of  
 143 change in surface loading will impact melt production more strongly such that small mag-  
 144 nitude but rapid deglaciation events, for example at  $\sim$ 85 ka, have a relatively large ef-  
 145 fect on eruption rates (Figure 2c).

146 The impact of deglaciation events is modulated by the upwelling rate of the solid  
 147 mantle because the upwelling rate controls the background productivity of the melting  
 148 model. At slower upwelling rates, i.e.  $10 \text{ mm yr}^{-1}$ , some periods of deglaciation are not  
 149 recorded in the flux of magma erupted. An example of this is the warming event at 60 ka  
 150 (Figure 2), where the  $10 \text{ mm yr}^{-1}$  upwelling model produces no response in either the  
 151 eruption rate or  $\text{CO}_2$  flux. If however upwelling is more rapid,  $20 \text{ mm yr}^{-1}$ , then there  
 152 is a clear pulse in melt eruption rate (Figure 2). For a more productive scenario, there  
 153 is increased shallow melting. The displacement imposed by the flexural response to un-  
 154 loading dissipates with depth. Therefore, if melting is productive and hence shallow it  
 155 will feel the effects of the unloading to a greater extent when compared to a less produc-  
 156 tive melting system. Furthermore, when productivity is low, the porosity is low and the  
 157 rate of vertical melt flow is slow such that a pulse in melt production will not reach the  
 158 surface rapidly.

159 The magnitude of  $\text{CO}_2$  flux peaks are not linearly related to the magnitude in erup-  
 160 tion rates (Figure 2d). For example, in the  $20 \text{ mm yr}^{-1}$  upwelling rate model, the largest  
 161  $\text{CO}_2$  peak is estimated to occur at  $\sim$ 60 ka and not during the volumetrically larger mag-  
 162 matic pulse at the end of the Pleistocene (Figure 2d). This difference is because when  
 163 the  $\sim$ 60 ka warming occurred, the melt was enriched in carbon due to the preceding rapid  
 164 glaciation. Magma supplied from the mantle during the Late-Pleistocene pulse were more  
 165 depleted in carbon compared to those in the 60 ka event. The implication of this result  
 166 is that volumetrically small volcanic events might have just as a strong influence on  $\text{CO}_2$

167 degassing as the more significant periods of volcanic eruptions, and this is dependent on  
 168 the history of glacial forcing.

### 169 3.2 Glacial Forcing Through the Latest Pleistocene and Holocene

170 During the last 40 ka, our model suggest that CO<sub>2</sub> flux is highly dependent on the  
 171 glacial forcing. There are two distinct late Pleistocene magmatic pulses, separated by  
 172 the Younger Dryas cold period (Figure 3a and b). However, for the model M2 ice sheet  
 173 history there are three pulses in CO<sub>2</sub> flux at the end of the Pleistocene, due to the faster  
 174 ice sheet growth entering the LGM from 35 to 25 ka in this model (Figure 3a and e). This  
 175 peak in CO<sub>2</sub> flux is because the small magnitude but rapid deglaciations after 25 ka tap  
 176 melts rich in trace elements including Nb and carbon (Figure 3c and d).

177 The observed time series of incompatible trace element concentrations in Icelandic  
 178 magmas and ice sheet history have been suggested to be strongly associated (Eason et  
 179 al., 2015; Gee et al., 1998; Jull & McKenzie, 1996; MacLennan et al., 2002; Sinton et al.,  
 180 2005). Of these studies Gee et al. (1998) and Eason et al. (2015) report on the Nb com-  
 181 position of lavas erupted and give age ranges for the erupted lavas. Dating lava flow in  
 182 Iceland is complex given the lack of reliable markers from which ages can be obtained.  
 183 This means that ages are instead typically taken from the morphology and tephrochronol-  
 184 ogy of erupted flows (MacLennan et al., 2002), which is subjective and open to debate.  
 185 We therefore must take the age ranges for the Nb compositions reported by Gee et al.  
 186 (1998) and Eason et al. (2015) as indicative. We therefore chose to bin the ages into 2.5 kyr  
 187 intervals from 0 to 17.5 ka and then at 5 kyr intervals (Figure 3c). The reduction in Nb  
 188 compositions plotted is in line with the trends observed within the more selective La and  
 189 Sm data set presented in MacLennan et al. (2002), and is therefore likely robust.

190 We find that the predicted change in Nb, which behaves in a similar way to C dur-  
 191 ing mantle melting (Rosenthal et al., 2015; Saal et al., 2002), from all our models fit within  
 192 the range of the observations (Figure 3c). The M2 model gives the strongest signature  
 193 in Nb concentrations of deglaciation during the end of the Pleistocene, while the signa-  
 194 ture is more subdued in the M1 ice sheet model (Figure 3c). The 1D forward model used  
 195 is highly idealised, and yet the agreement between the observations and model is encour-  
 196 aging, and suggests the compositional change observed in lavas erupted during the late-  
 197 Pleistocene to early Holocene is due to rapid deglaciation (Eason et al., 2015; Gee et al.,  
 198 1998; MacLennan et al., 2002; Sinton et al., 2005). This implies that the observed change  
 200 in melt composition is due to change in ice sheet loading and that the pre-deglaciation  
 201 volcanism likely released a significant volume of CO<sub>2</sub> (Figure 3e).

201 The 1D column model will underestimate the impact of change in deep melt pro-  
 202 ductivity, as it cannot capture the deep wings of the zone of partial melting. To explore  
 203 the impact of this we force a series of 1D models with the vertical flow taken from steady  
 204 state corner flow perturbed by the flexural response of the deglaciation of a 200 km wide  
 205 ice sheet. The half spreading rate is assumed to be 10 mm yr<sup>-1</sup>, and the mantle poten-  
 206 tial temperature is 1450 °C. Melt travels vertically from the zone of partial melting in  
 207 columns at 0 to 80 km from the rift axis (Figure 4). The steady state thickness of melt  
 208 erupted at the surface of the simplified 2D model is 15 km, and glacial forcing causes this  
 209 thickness to vary around this value by the order of 10 km except for a large spike at the  
 210 LGM (Figure NEW). The crust of Iceland varies in thickness from 20 to 40 km (e.g. Jenk-  
 211 ins et al., 2018), and therefore a model steady state thickness of 15 km is a reasonable  
 212 lower end-member prediction given that the crust is made of extrusions and intrusions.

213 After glacial perturbation we find that in the central zone, from the ridge centre  
 214 to 40 km distance, the trend in Nb and CO<sub>2</sub> flux is relatively similar, with a reduction  
 215 in Nb at 15 ka. At distances greater than 40 km, a peak in Nb and CO<sub>2</sub> flux is predicted  
 216 to occur with an increasing delay compared to the centre of extension (Figure 4). This  
 217 delay is due to the greater distance that the melt has to travel along the vertical path

from the top of the melt zone to the surface at increasing distance from the centre of extension. In full 2D models the distal melt will pool as it migrates laterally towards the centre of extension (Katz, 2008), yet the difference in ascent velocity due to the increase porosity as the melt pools would likely not be sufficient to overcome the increased distance that the signal will have to travel.

The full solution to the coupled equations of magma dynamics would suggest that melts generated at a distance of up to 60 km from the centre of extension are advected to the ridge axis (Katz, 2008). If all of the melt generated up to 60 km from the centre of extension is erupted, then the CO<sub>2</sub> flux is significantly increased during the Holocene due to the addition input of melt from the distal parts of the zone of partial melting (Figure 4b). Therefore these low productivity and deep regions of the zone of partial melting might be a key exporter of mantle carbon into the atmosphere. However, the range of observed Nb concentrations are relatively similar to the axial concentrations, from within <40 km of the rift centre (Figure 4). This would suggest that the widest regions of the zone of partial melting are not sampled by the volcanism in the Reykjanes Ridge and Western Volcanic Zone, leading to an estimate of CO<sub>2</sub> fluxes more in line with the simpler 1D model.

## 4 Discussion and Conclusions

The models imply that the deglaciation beginning at 18 ka and continuing through the Bolling warming at 14.8 ka released substantial quantities of CO<sub>2</sub> when compared to the last 120 ka (Figure 3c and Figure 4b), and this elevated CO<sub>2</sub> release was because of the preceding growth of the ice sheet. Volcanism during this time would have taken place in a sub-glacial environment and unsurprisingly does not feature in the post-glacial sub-aerial record. Evidence from sub-glacial volcanic units (tuyas) erupted during this time period (Hartley, Thordarson, & de Joux, 2016) suggest volumetric and compositional trends consistent with those predicted by our model (Figure 3c and Figure 4).

Forcing our model with the long-term 120 ka ice sheet history produces a periodic fluxing of CO<sub>2</sub> from Icelandic volcanoes due to ice-loss events over this period, implying a close link between ice dynamics and magmatic out-gassing. The greatest release of CO<sub>2</sub>, however, occurred during the period of ice-loss just before the Younger Dryas (~14 ka), and therefore before the largest phase of late-Pleistocene deglaciation (Figure 4). The concentration of CO<sub>2</sub> released in this magmatic pulse was enhanced due to the lack of any significant loss of ice volume since ~40 ka. This created a magmatic system capable of fluxing large volumes of carbon during the initial period of post-LGM deglaciation (both models M1 and M2, Figure 3e), possibly contributing to the increased atmospheric CO<sub>2</sub> levels thought to be recorded between 15 and 14 ka in the EPICA Dome C ice core (Köhler, Knorr, Buiiron, Lourantou, & Chappellaz, 2011). It is therefore possible that this pulse of magmagenic CO<sub>2</sub>, from Iceland and elsewhere (e.g. /citephuybers-2009, bolstered the climate warming, and final phase of deglaciation, that proceeded the Younger Dryas.

The CO<sub>2</sub> flux due to deglaciation is strongly influenced by the ice sheet history. Mantle CO<sub>2</sub> flux does not follow a linear relationship with eruption rates: large peaks in CO<sub>2</sub> are also predicted for periods in time when the volume flux is not very high (Figure 2d and 3e). In effect we cannot conclude that all deglaciation events, or other rapid unloading events due to for example erosion (e.g. Sternai, Caricchi, Castelltort, & Chambagnac, 2016), lead to a large flux of volatile gases into the Earths atmosphere. The Earth system is more complex than such simple causality, yet one clear implication is that deglaciation after a prolonged period of ice-house conditions will lead to a significant carbon degassing of the upper mantle.

267 **Supporting Information**

268 A detailed discussion of the methodology can be found in the supporting informa-  
 269 tion (Andersen et al., 2004; Andrews, 2008; Armitage, Collier, Minshull, & Henstock, 2011;  
 270 Clark et al., 2009; Geirsdóttir, 2011; Gibson & Geist, 2010; Gurenko & Chaussidon, 1995;  
 271 Katz, Spiegelman, & Langmuir, 2003; Lambeck & Chappel, 2001; Lambeck, Rouby, Pur-  
 272 cell, Sun, & Sambridge, 2014; McKenzie & O’Nions, 1991; Miller, Zhu, Montési, & Gae-  
 273 tani, 2014; Ribe, 1985; Scott, 1992; Shorttle & Maclennan, 2011; Silbeck, 1975; Sleep &  
 274 Snell, 1976; Spiegelman, 1996; Spratt & Lisicki, 2016).

275 **Acknowledgments**

276 We would like to thank M. A. Mary Gee (The University of Western Australia) for shar-  
 277 ing her Nb composition data from the Reykjanes Peninsula, and Tamara Pico (Harvard  
 278 University) for sharing her sea level curves. John J. Armitage acknowledges funding from  
 279 an Agence National de la Recherche (France), Accueil de Chercheurs de Haute Niveau,  
 280 grant InterRift. The 1-D melting model is available from <https://bitbucket.com/johnjarmitage/melt1d-icesheet/>

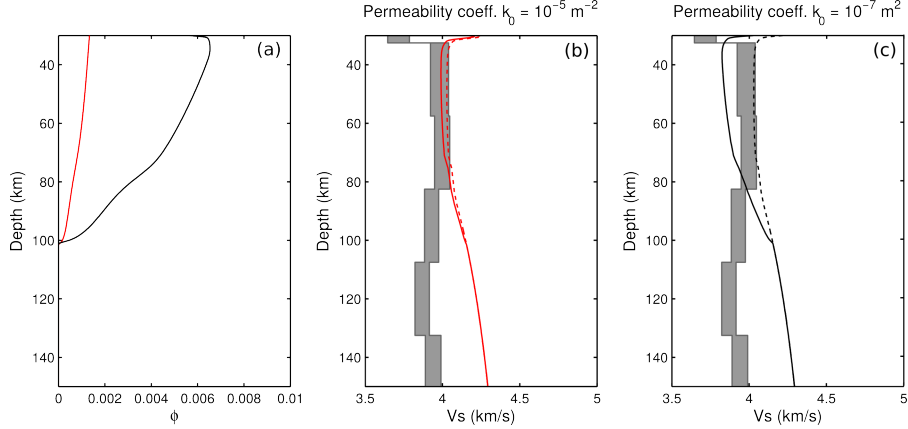
282 **References**

- 283 Andersen, K. K., Azuma, N., Barnola, J. M., Bigler, M., Biscaye, P., Caillon, N.,  
 284 ... White, J. W. C. (2004). High-resolution record of northern hemisphere  
 285 climate extending into the last interglacial period. *Nature*, *431*, 174-151. (doi:  
 286 10.1038/nature02805)
- 287 Andrews, J. T. (2008). The role of the Iceland Ice Sheet in the North Atlantic dur-  
 288 ing the late Quaternary: a review and evidence from Denmark Strait. *Journal*  
 289 *of Quaternary Science*, *23*, 3-20. (doi: 10.1002/jqs.1142)
- 290 Armitage, J. J., Collier, J. S., Minshull, T. A., & Henstock, T. J. (2011). Thin  
 291 oceanic crust and flood basalts: India-Seychelles breakup. *Geochemistry Geo-  
 292 physics Geosystems*, *12*(Q0AB07). (doi:10.1029/2010GC003316)
- 293 Burley, J. M. A., & Katz, R. F. (2015). Variations in mid-ocean ridge CO<sub>2</sub> emis-  
 294 sions driven by glacial cycles. *Earth and Planetary Science Letters*, *426*, 246-  
 295 258. (doi: 10.1016/j.epsl.2015.06.031)
- 296 Clark, P. U., Dyle, A. S., Shakun, J. D., Carlson, A. E., Clark, J., Wohlfarth, B., ...  
 297 McCabe, A. M. (2009). The last glacial maximum. *Science*, *325*, 710. (doi:  
 298 10.1126/science.1172873)
- 299 Crowley, J. W., Katz, R. F., Huybers, P., Langmuir, C. H., & Park, S. H. (2015).  
 300 Glacial cycles drive variations in the production of oceanic crust. *Science*, *347*,  
 301 1237-1240. (doi: 10.1126/science.1261508)
- 302 Dasgupta, R., & Hirschmann, M. M. (2010). The deep carbon cycle and melting  
 303 in Earth’s interior. *Earth and Planetary Science Letters*, *298*, 1-13. (doi:  
 304 10.1016/j.epsl.2010.06.039)
- 305 Eason, D. E., Sinton, J. M., Gronvöld, K., & Kurz, M. D. (2015). Effects of  
 306 deglaciation on the petrology and eruptive history of the Western Volcanic  
 307 Zone, Iceland. *Bulletin of Volcanology*, *77*(47). (doi: 10.1007/s00445-015-0916-  
 308 0)
- 309 Elliot, T., & Spiegelman, M. (2014). Melt migration in oceanic crustal production:  
 310 A u-series perspective. In *Treatise on geochemistry* (2nd ed., p. 543-581). Else-  
 311 vier. (doi: 10.1016/B978-0-08-095975-7.00317-X)
- 312 Gee, M. A. M., Taylor, R. N., Thirwall, M., & Murton, B. J. (1998). Glacioisostacy  
 313 controls chemical and isotopic characteristics of tholeiites from the Reykjanes  
 314 Peninsula, SW Iceland. *Earth and Planetary Science Letters*, *164*, 1-5.
- 315 Geirsdóttir, A. (2011). Pliocene and pleistocene glaciations of iceland: a brief  
 316 overview of the glacial history. In J. Ehlers, P. L. Gibbard, & P. Hughes  
 317 (Eds.), *Quaternary glaciations - extent and chronology, a closer look* (Vol. 15,

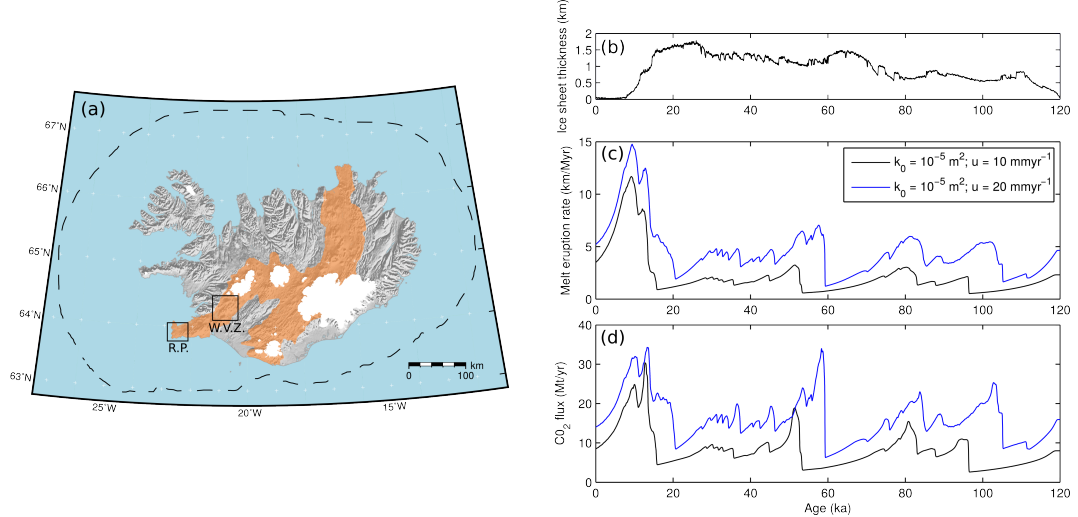
- 318 p. 199-210). Elsevier. (doi: 10.1016/B978-0-444-53447-7.00016-7)
- 319 Gibson, S. A., & Geist, D. (2010). Geochemical and geophysical estimates of litho-  
320 spheric thickness variation beneath galápagos. *Earth and Planetary Science  
Letters*, *300*, 275-286. (doi: 10.1016/j.epsl.2010.10.002)
- 321 Glazner, A. F., Manley, C. R., Marron, J. S., & Rojstaczer, S. (1999). Fire  
322 or ice: Anticorrelation of volcanism and glaciation in california over the  
323 past 800,000 years. *Geophysical Resaerch Letters*, *26*, 1759-1762. (doi:  
324 10.1029/1999GL900333)
- 325 Goes, S., Armitage, J. J., Harmon, N., Huismans, R., & Smith, H. (2012). Low seis-  
326 mic velocities below mid-ocean ridges: Attenuation vs. melt retention. *Journal  
327 of Geophysical Research*, *117*, B12403. (doi: 10.1029/2012JB009637)
- 328 Gurenko, A. A., & Chaussidon, M. (1995). Enriched and depleted primitive melts  
329 included in olivine from icelandic tholeiites: Origin by continuous melting of a  
330 single mantle column. *Geochimica et Cosmochimica Acta*, *59*, 2905-2917.
- 331 Hammond, W. C., & Humphreys, E. D. (2000). Upper mantle seismic wave ve-  
332 locity: Effects of realistic partial melt geometries. *Journal of Geophysical Re-  
333 search*, *105*, 10975-10986.
- 334 Harmon, N., & Rychert, C. A. (2016). Joint inversion of teleseismic and ambient  
335 noise Rayleigh waves for phase velocity maps, an application to Iceland. *Jour-  
336 nal of Geophysical Research*, *121*, 5966-5987. (doi: 10.1002/2016JB012934)
- 337 Hartley, M. E., Thordarson, T., & de Joux, A. (2016). Postglacial eruptive history  
338 of the Askja region, North Iceland. *Bulleting of Volcanology*, *78*(28). (doi:  
339 10.1007/s00445-016-1022-7)
- 340 Huybers, P., & Langmuir, C. H. (2009). Feedback between deglacation, volca-  
341 nism, and atmospheric CO<sub>2</sub>. *Earth and Planetary Science Letters*, *286*, 479-491.  
342 (doi: 10.1016/j.epsl.2009.07.014)
- 343 Huybers, P., & Langmuir, C. H. (2017). Delayed CO<sub>2</sub> emissions from mid-ocean  
344 ridge volcanism as a possible cause of late-Pleistocene glacial cycles. *Earth and  
345 Planetary Science Letters*, *457*, 238-249. (doi: 10.1016/j.epsl.2016.09.021)
- 346 Jellinek, M. A., Mange, M., & Saar, M. O. (2004). Did melting glaciers  
347 cause volcanic eruptions in eastern california? probing the mechanisms  
348 of dike formation. *Journal of Geophysical Research*, *109*(B09206). (doi:  
349 10.1029/2004JB002978)
- 350 Jenkins, J., Maclennan, J., Green, R. G., Cottaar, S., Deuss, A. F., & White, R. S.  
351 (2018). Crustal formation on a spreading ridge above a mantle plume: Re-  
352 ceiver function imaging of the Icelandic crust. *Journal of Geophysical Re-  
353 search*, *123*, 5190-5208. (doi: 10.1029/2017JB015121)
- 354 Jull, M., & McKenzie, D. (1996). The effect of deglaciation on mantle melting be-  
355 neath Iceland. *Journal of Geophysical Research*, *101*(B10), 21815-21828.
- 356 Katz, R. F. (2008). Magma dynamics with the enthalpy method: Benchmark so-  
357 lutions and magmatic focusing at mid-ocean ridges. *Journal of Petrology*, *49*,  
358 2099-2121. (doi:10.1093/petrology/egn058)
- 359 Katz, R. F., Spiegelman, M., & Langmuir, C. H. (2003). A new parameterization of  
360 hydrous mantle melting. *Geochemistry Geophysics Geosystems*, *4*, 1073. (doi:  
361 10.1029/2002GC000433)
- 362 Köhler, P., Knorr, G., Buiron, D., Lourantou, A., & Chappellaz, J. (2011). Abrupt  
363 rise in atmospheric CO<sub>2</sub> at the onset of the Bolling/Allerod: in-situ ice core  
364 data versus true atmospheric signals. *Climate of the Past*, *7*, 473-486. (doi:  
365 10.5194/cp-7-473-2011)
- 366 Lambeck, K., & Chappel, J. (2001). Sea level change through the last glacial cycles.  
367 *Science*, *292*, 679-686. (doi: 10.1126/science.1059549)
- 368 Lambeck, K., Rouby, H., Purcell, A., Sun, Y., & Sambridge, M. (2014). Sea level  
369 and global ice volumes from the Last Glacial Maximum to the Holocene.  
370 *Proceedings of the National Academy of Sciences*, *111*, 15296-15303. (doi:  
371 10.1073/pnas.141176211)

- 373 Lund, D. C., & Asimow, P. D. (2011). Does sea level influence mid-ocean ridge mag-  
 374 matism on Milankovitch timescales? *Geochemistry Geophysics Geosystems*,  
 375 12(Q12009). (doi: 10.1029/2011GC003693)
- 376 Maclennan, J., Jull, M., McKenzie, D., Slater, L., & Gronvöld, K. (2002). The  
 377 link between volcanism and deglaciation in Iceland. *Geochemistry Geophysics  
 378 Geosystems*, 3(11, 1062). (doi: 10.1029/2001GC000282)
- 379 McKenzie, D., & O'Nions, R. K. (1991). Partial melt distribution from inversion of  
 380 rare earth element concentrations. *Journal of Petrology*, 32, 1021-1091.
- 381 Miller, K. J., Zhu, W., Montési, L. G. J., & Gaetani, G. A. (2014). Experimental  
 382 quantification of permeability of partially molten mantle rock. *Earth and Plan-  
 383 etary Science Letters*, 388, 273-282. (doi: 10.1016/j.epsl.2013.12.003)
- 384 Nordahl, H., & Ingólfsson, O. (2015). Collapse of the Icelandic ice sheet controlled  
 385 by sea level rise? *Arktos*, 1, 1-13. (doi: 10.1007/s41063-015-0020-x)
- 386 Pagli, C., & Sigmundsson, F. (2008). Will present day glacier retreat increase  
 387 volcanic activity? stress induced by recent glacier retreat and its effect on  
 388 magmatism at the Vatnajökull ice cap, Iceland. *Geophysical Research Letters*,  
 389 35(L09304). (doi: 10.1029/2008GL033510)
- 390 Patton, H., Hubbard, A., Bradwell, T., & Schomackere, A. (2017). The configura-  
 391 tion, sensitivity and rapid retreat of the Late Weichselian Icelandic ice sheet.  
 392 *Earth-Science Reviews*, 166, 223-245. (doi: 10.1016/j.earscirev.2017.02.001)
- 393 Peltier, W. R. (2004). Global glacial isostacy and the surface of the ice-age Earth:  
 394 The ICE-5G (VM2) model and grace. *Annual Reviews of Earth and Planetary  
 395 Science*, 32, 111-149. (2004)
- 396 Pico, T., Creveling, J. R., & Mitrovica, J. X. (2017). Sea-level records from the  
 397 U.S. mid-Atlantic constrain Laurentide Ice Sheet extent during Marine Isotope  
 398 Stage 3. *Nature Communications*, 8(15621). (doi: 10.1038/ncomms15612)
- 399 Rawson, H., Pyle, D. M., Mather, T. A., Smith, V. S., Fontijn, K., Lachowycz,  
 400 S. M., & Naranjo, J. A. (2016). The magmatic and eruptive response of arc  
 401 volcanoes to deglaciation: Insights from southern Chile. *Geology*, 44, 251-254.  
 402 (doi: 10.1130/G37504.1)
- 403 Ribe, N. M. (1985). The generation and composition of partial melts in the earth's  
 404 mantle. *Earth and Planetary Science Letters*, 73, 361-376.
- 405 Rosenthal, A., Hauri, E. H., & Hirschmann, M. M. (2015). Experimental determi-  
 406 nation of C, F, and H partitioning between mantle minerals and carbonated  
 407 basalt, CO<sub>2</sub>/Ba and CO<sub>2</sub>/Nb systematics of partial melting, and the CO<sub>2</sub>  
 408 contents of basaltic source regions. *Earth and Planetary Science Letters*, 415,  
 409 77-87. (doi: 10.1016/j.epsl.2014.11.044)
- 410 Saal, A. E., Hauri, E. H., Langmuir, C. H., & Perfit, M. R. (2002). Vapour un-  
 411 dersaturation in primitive mid-ocean-ridge basalt and the volatile content of  
 412 Earths upper mantle. *Nature*, 419, 451-455. (doi: 10.1038/nature01073)
- 413 Schmidt, P., Lund, B., Hieronymus, C., Maclennan, J., Arnadottir, T., & Pagli,  
 414 C. (2013). Effects of present-day deglaciation in Iceland on mantle melt  
 415 production rates. *Journal of Geophysical Research*, 118, 3366-3379. (doi:  
 416 10.1002/jgrb.50273)
- 417 Scott, D. R. (1992). Small-scale convection and mantle melting beneath mid-ocean  
 418 ridges. In J. Phipps Morgan, D. K. Blackman, & J. M. Sinton (Eds.), *Mantle  
 419 flow and melt generation at mid-ocean ridges* (Vol. Geophysical Monograph 71,  
 420 p. 327-352). American Geophysical Union.
- 421 Shorttle, O., & Maclennan, J. (2011). Compositional trends of icelandic  
 422 basalts: Implications for short-length scale lithological heterogeneity in  
 423 mantle plumes. *Geochemistry Geophysics Geosystems*, 12, Q11008. (doi:  
 424 10.1029/2011GC003748)
- 425 Sigvaldson, G. E., Annertz, K., & Nilsson, M. (1992). Effect of glacier load-  
 426 ing/delowering on volcanism: postglacial volcanic production rate of the Dyn-  
 427 gjufjöll area, central Iceland. *Bulletin of Volcanology*, 54, 385-392. (doi:

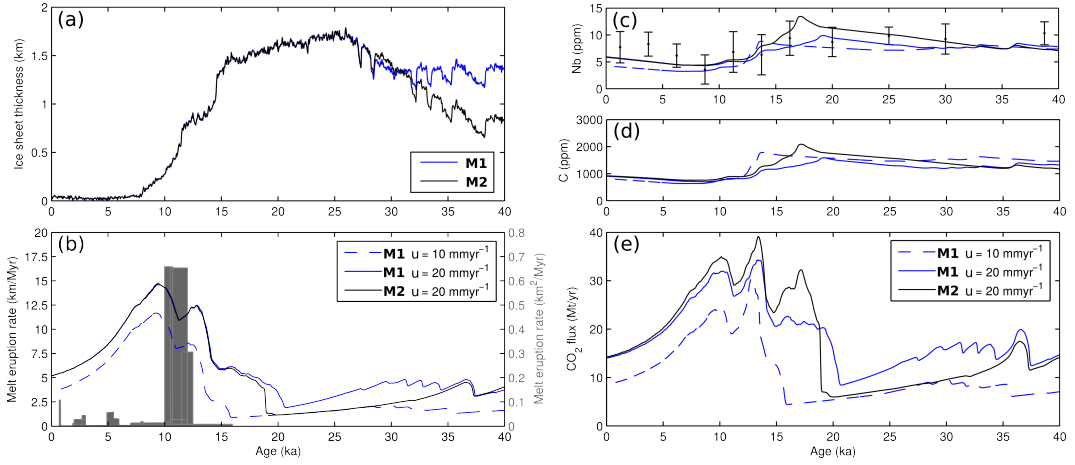
- 428 10.1007/BF00312320)
- 429 Silbeck, J. N. (1975). On the fluid dynamics of ridge crests. In *Notes on the 1975*  
430 *summer study program in geophysical fluid dynamics at the Woods Hole oceanographic*  
431 *institution*, (Vol. 2, p. 113-122).
- 432 Sinton, J., Grönvold, K., & Saemundsson, K. (2005). Postglacial eruptive history  
433 of the Western Volcanic Zone, Iceland. *Geochemistry Geophysics Geosystems*,  
434 6(Q12006). (doi: 10.1029/2005GC001021)
- 435 Sleep, N. H., & Snell, N. S. (1976). Thermal contraction and flexure of mid-  
436 continent and Atlantic marginal basins. *Geophysical Journal of the Royal*  
437 *Astronomical Society*, 45, 125-154.
- 438 Spiegelman, M. (1996). Geochemical consequences of melt transport in 2-D: The  
439 sensitivity of trace elements to mantle dynamics. *Earth and Planetary Science*  
440 *Letters*, 139, 115-132.
- 441 Spratt, R. M., & Lisiecki, L. E. (2016). A late Pleistocene sea level stack. *Climate of*  
442 *the Past*, 12, 1079-1092. (doi: 10.5194/cp-12-1079-2016)
- 443 Sternai, P., Caricchi, L., Castelltort, S., & Champagnac, J. D. (2016). Deglaciation  
444 and glacial erosion: A joint control on magma productivity by continental unloading.  
445 *Geophysical Research Letters*, 43, 1632-1641. (doi:  
446 10.1002/2015GL067285)
- 447 Wasylenski, L. E., Baker, M. B., Kent, A. J. R., & Stopler, E. M. (2003). Near-  
448 solidus melting of the shallow upper mantle: partial melting experiments on  
449 depleted peridotite. *Journal of Petrology*, 44, 116-1191.



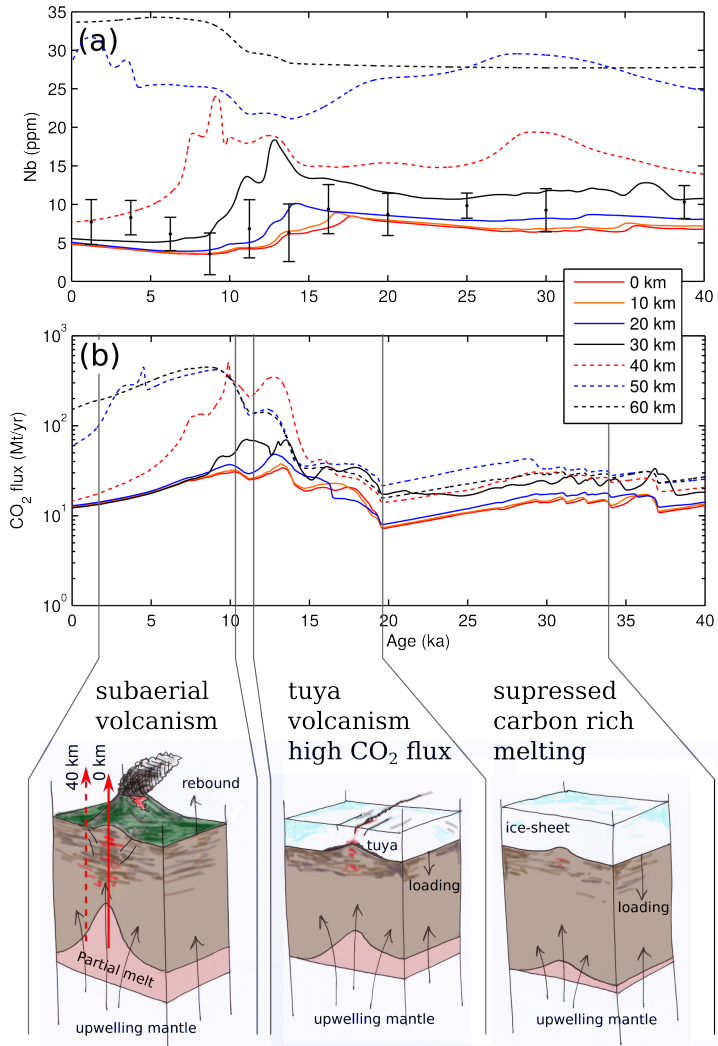
450 **Figure 1.** Profiles of porosity and S-wave seismic velocity for the two model permeabilities of  
 451  $k_0 = 10^{-7} \text{ m}^2$  black line, and  $k_0 = 10^{-5} \text{ m}^2$  red line. (a) Porosity plotted against depth at steady  
 452 state. (b) S-wave velocity from the joint inversion of teleseismic and ambient noise Rayleigh  
 453 waves (Harmon & Rychert, 2016) and the predicted S-wave profile from the high permeability  
 454 case. The model includes the addition of the adiabatic gradient, the anharmonic effects from the  
 455 mineralogy and effects of attenuation (Goes et al., 2012). The dashed line assumes melt has no  
 456 effect, the solid line includes a 7.9 % reduction in  $V_S$  per percent melt (Hammond & Humphreys,  
 457 2000). (c) S-wave velocity predictions for the low permeability case.



458 **Figure 2.** Response of the model to periodic and observed ice sheet thickness changes of the  
 459 last 120 ka. (a) Map of Iceland showing the locations of the volcanic rift zones in orange and the  
 460 maximum extent of the ice sheet at the last glacial maximum (dashed line). The boxes show the  
 461 location of the Reykjanes Peninsular (R. P.) and the Western Volcanic Zone (W. V. Z.). (b) The  
 462 ice sheet thickness predicted from the ice sheet model M1 over the last 120 ka. (c) Melt eruption  
 463 rate and (d) carbon flux response to the step change in ice sheet thickness: black line, an upper  
 464 mantle permeability coefficient of  $k_0 = 10^{-5} \text{ m}^2$  and upwelling velocity of  $10 \text{ mm yr}^{-1}$ , and blue  
 465 line, an upwelling velocity of  $20 \text{ mm yr}^{-1}$ .



466 **Figure 3.** Impact of ice sheet growth and decay on melt eruption and composition over the  
467 last 40 ka. (a) Ice sheet models M1 and M2 taken from the sea-level models of Peltier (2004) and  
468 Pico et al. (2017) respectively. (b) Melt eruption rates (in km of melt per Myr): blue solid line,  
469 ice sheet history 5G for  $k_0 = 10^{-5} \text{ m}^2$  with an upwelling rate of  $20 \text{ mm yr}^{-1}$ ; blue dashed line, M1  
470 for  $k_0 = 10^{-5} \text{ m}^2$  with an upwelling rate of  $10 \text{ mm yr}^{-1}$ ; black solid line, ice sheet history M2 for  
471  $k_0 = 10^{-5} \text{ m}^2$  with an upwelling rate of  $20 \text{ mm yr}^{-1}$ . The gray region shows estimated eruption  
472 rates from geological observations (MacLennan et al., 2002)] (in  $\text{km}^2$  of melt per Myr). (c) Ob-  
473 served and predicted Nb concentrations (ppm), observations are from the Reykjanes Peninsula  
474 and the Western Volcanic Zone (Eason et al., 2015; Gee et al., 1998; Sinton et al., 2005) and are  
475 binned at 2.5 kyr intervals from 0 to 17.5 ka and then at 5 kyr intervals. (d) Predicted variation of  
476 in the concentration of carbon (ppm) within the erupted melt. (e) Predicted variation in the flux  
477 of  $\text{CO}_2$ , assuming that the flux of  $\text{CO}_2$  that Icelandic volcanism covers an area of  $30,000 \text{ km}^2$ , and  
478  $\text{CO}_2 (\text{ppm}) = 3.67 \text{ C (ppm)}$  (see Eq. 23 in the Supplementary Material).



479 **Figure 4.** Impact of glacial history on off-axis and on-axis melting. A series of 1D column  
 480 melting models forced by the response to deglaciation (ice sheet history model M1) where the  
 481 mantle flow is of steady state corner flow. (a) Nb concentrations from the centre of extension out  
 482 to 60 km from the centre of extension. The mean concentration weighted by the eruption rate is  
 483 plotted as the thick black line. (b) Predicted CO<sub>2</sub> flux from the series of vertical melting models.  
 484 The late-Pleistocene eruptions are typified by tuya magmatism. This will have been the case up  
 485 until at least ~14 ka, where either magmatism was suppressed or when eruptions occurred they  
 486 will have been beneath at least 1 km of ice-cover (Hartley et al., 2016). The suppressed melting  
 487 regime will have become carbon rich because the shallow low-C melt production is damped due  
 488 to the ice-sheet loading. Upon deglaciation there is increased volcanism, which initially taps the  
 489 melt rich carbon.